ARTICLE IN PRESS

Available online at www.sciencedirect.com

ScienceDirect

Ceramics International ▮ (▮▮▮▮) ▮▮▮–▮▮▮

CERAMICS INTERNATIONAL

www.elsevier.com/locate/ceramint

Green synthesis of aniline by phosphorus-doped titanium dioxide polymorphs

R.M. Mohamed[a,b,c,*], Mohammad W. Kadi[a]

[a]Department of Chemistry, Faculty of Science, King Abdulaziz University, P.O. Box 80203, Jeddah 21589, Kingdom of Saudi Arabia
[b]Advanced Materials Department, Central Metallurgical R&D Institute, CMRDI, P.O. Box 87 Helwan, Cairo 11421, Egypt
[c]Center of Excellence in Environmental Studies, King Abdulaziz University, P.O. Box 80216, Jeddah 21589, Saudi Arabia

Received 15 November 2013; received in revised form 22 November 2013; accepted 22 November 2013

Abstract

Phosphor doping in association with a heterostructure not only modifies the band structure of titanium dioxide (TiO_2) to make it more responsive to visible light, but it also suppresses its charge recombination and causes TiO_2 to have enhanced photoactivity. In this paper, we report on the controlled synthesis of phosphor-doped binary and ternary TiO_2 nanostructures through a hydrothermal method. The phase and morphology of the samples can be tuned by simply changing the hydrothermal time. Also, the visible-light photoactivity of the samples was evaluated by the reduction of nitrobenzene. The as-prepared catalysts exhibit enhanced photocatalytic activity in comparison to P_{25} and the undoped counterpart, and the selected catalyst shows high photostability and photoactivity after reuse five times. These new TiO_2 nanostructures present a promising candidate for application in photocatalysis, photochemistry, sensors, and solar cells.

Keywords: TiO_2 polymorphs; Phosphor doping; Visible photocatalysis; Aniline synthesis

1. Introduction

The catalytic hydrogenation method has been commonly used to reduce nitrobenzene (NB) to aniline, which is one of the most important chemicals and intermediates in the production of pharmaceuticals, dyes, pigments, and pesticides [1,2] within industrial and laboratory environments. Transition metals (Cu and Ni) and noble metals (Pt, Pd and Au) are commonly used as the catalyst [1–3] and the reaction must be performed at a high temperature, a high H_2 pressure, and a long time in order to reach a satisfactory selectivity of aniline [3,4]. A photochemical-induced reduction of nitrobenzene into aniline, which can occur at room temperature with the use of a photocatalyst, has important scientific value and attracts extensive attention in view of pursuing environmentally benign or green synthesis [5–7]. Although the reduction of nitrobenzene (NB) and its derivatives to aniline through the use of photocatalytic technology has been reported in some literature [5,8–10], the conversion and selectivity are low and TiO_2 is commonly used as the photocatalyst [8,11–14]. However, TiO_2 can only be activated by UV light. Therefore, only about 3%–5% of the solar spectrum light can be used by TiO_2. From the viewpoint of solar-energy utilization, visible-light-excited photocatalysts should be developed. For a semiconductor photocatalyst, the more negative the value of the conduction band it possesses, the stronger the reduction activity can be expected. In theory, when the conduction band potential of a photocatalyst is lower than -0.486 V, nitrobenzene can be photocatalytically reduced into aniline ($E(C_6H_5NO_2/C_6H_5NH_2) = -0.486$ V [15], vs. NHE). Therefore, designing new narrow-band-gap semiconductor photocatalysts that have high negative values of the conduction band may be an effective method for the reduction of NB. As a wide-bandgap semiconducting material, TiO_2 responds only in the ultraviolet (UV) region. This limits even wider applications of TiO_2 under visible light irradiation that accounts for a major part of solar

*Corresponding author at: Department of Chemistry, Faculty of Science, King Abdulaziz University, P.O. Box 80203, Jeddah 21589, Kingdom of Saudi Arabia. Tel.: +96 65 4071 5648; fax: +96 62 695 2292.
E-mail address: mhmdouf@gmail.com (R.M. Mohamed).

0272-8842/$ - see front matter © 2013 Elsevier Ltd and Techna Group S.r.l. All rights reserved.
http://dx.doi.org/10.1016/j.ceramint.2013.11.115

Please cite this article as: R.M. Mohamed, M.W. Kadi, Green synthesis of aniline by phosphorus-doped titanium dioxide polymorphs, Ceramics International (2013), http://dx.doi.org/10.1016/j.ceramint.2013.11.115

energy (~45%) [16]. To date, many strategies, such as doping, metal-loading, and sensitizing approaches, have been designed to shift the absorption onset of TiO_2 from UV to the visible light region [17–25]. Although encouraging progress has been made in recent years, limitations still exist in the consideration of thermal stability [26,27], cost [28,29], and photochemical stability [30,31] of the TiO_2-based nanomaterials. Recently, a new type of hetero-structured $FeTiO_3/TiO_2$ photocatalyst [32,33] that appears to have good photochemical stability during reuse under visible light irradiation has been demonstrated for the efficient decomposition of the organic compounds; however, its photocatalytic efficiency is not higher than that of pure TiO_2 or TiO_2 Degussa P_{25} when working under simulated sunlight [32]. TiO_2 mainly has three polymorphs (anatase, brookite, and rutile) with different band structures [34]. Despite the fact that heterostructures that comprise two forms of titania can endure photocorrosion, the composites exhibit enhanced activity only under irradiation by UV light and/or simulated sunlight [35–38]. Recently, a strategy combining heterostructure with nitrogen doping has been demonstrated for synthesizing anatase/rutile nanostructures with 9-fold visible light activity in comparison to P_{25} [39]. Although different opinions currently remain regarding the fundamental mechanism with respect to charge transfer [38–40], it is well-accepted that the heterostructures, or even mixtures of titania polymorphs, can inhibit charge recombination and enable enhanced photocatalytic efficiency [38,39]. Also, recent studies have shown that one-dimensional (1D), single-crystalline TiO_2 nanostructures, such as tubes [30,34], wires [30], and belts [41], retain a high specific surface area but have a lower charge carrier recombination rate in comparison with their spherical counterparts. In this work, we reported a facile hydrothermal method to synthesize phosphors-incorporated TiO_2 polymorphs with a tunable anatase/rutile/brookite ratio. The ratios of anatase to rutile to brookite in mixed-phase TiO_2 nanocrystals could be easily tuned by simply changing the hydrothermal time. To confirm the effect of mixed anatase, rutile, and brookite phases on the photocatalytic activity, the performance of prepared TiO_2 samples was achieved for the photoreduction of nitrobenzene to aniline under visible light irradiation.

2. Experimental section

2.1. Preparation of TiO_2 nanospheres

Analytical-grade tetra-n-butyl titanate (TBT), isopropanol, concentrated nitric acid (63%–65%), and hypophosphrous acid were used directly without further purification. TiO_2 nanospheres were prepared by the following method: a three-neck flask (100 mL) containing 20 mL of distilled water was fixed to a cryogenic thermostat. The water was cooled to 2 °C and acidified by adding 30 mL of concentrated HNO_3 under vigorous agitation, followed by the dropwise addition of a solution containing 3 mL of TBT and 30 mL of isopropanol with continuous stirring for 12 h. The mixture was filtrated and the precipitate was washed several times with distilled water in order to obtain TiO_2 nanospheres (T).

2.2. Preparation of phosphors-doped TiO_2 polymorphs

In a typical preparation procedure, the as-obtained TiO_2 nanospheres were mixed with 20 mL of hypophosphrous acid, followed by ultrasonic treatment at room temperature for 20 min to form a latex suspension. The suspension was transferred into a Teflon-lined autoclave (50 mL capacity). The autoclave was heated to 200 °C for 12–48 h and allowed to cool to room temperature. The precipitate was collected by filtration, washed thoroughly with distilled water and anhydrous ethanol, and finally dried in a vacuum oven. The phosphors-doped samples that resulted from heating at 200 °C for 12, 24, 36, and 48 h are designated as PT-12, PT-24, PT-36, and PT-48, respectively. In a control experiment, TiO_2 nanospheres were mixed with distilled water instead of hypophosphrous acid and heated at 200 °C for 36 h. The resulting undoped sample was denoted as T-36.

2.3. Characterization

The specific surface area of the prepared samples was evaluated from the adsorption–desorption isotherms of nitrogen at −196 °C that were detected by using Nova 2000 series apparatus (Chromatech). The specific surface areas of materials were calculated by using the BET method and by applying the Brunauer–Emmett–Teller (BET) equation. Prior to the measurements, all samples were degassed under vacuum at 150 °C for 2 h. Phase identification was determined from X-ray diffraction (XRD) analysis that was conducted at room temperature by employing a Bruker axis D8 instrument using Cu Kα radiation ($\lambda = 1.540$ Å). For the heterostructured samples, the weight fraction of every component can be calculated from Eqs. (1)–(3)

$$W_A = k_A I_A / k_A I_A + k_B I_B \quad (1)$$

$$W_B = k_B I_B / k_A I_A + k_B I_B \quad (2)$$

$$W_R = I_R / k_A I_A + k_B I_B + I_R \quad (3)$$

where W_A, W_B, and W_R separately represent the weight fraction of anatase, brookite, and rutile; coefficients k_A and k_B are 0.886 and 2.721 in sequence, and I_A and I_B denote the integrated intensity of the anatase (101) peak and the brookite (121) peak, respectively [42]. The surface morphology of all prepared catalysts was examined by using a transmission electron microscope (TEM) (JEOL-JEM-1230). Before loading into the TEM, the samples were suspended in ethanol, followed by ultrasonication for 30 min. The band-gap energies of the samples were determined by UV–visible, diffuse reflectance spectra (UV–vis-DRS) in air at room temperature in the wavelength range of 200–800 nm by using the UV/Vis/NIR spectrophotometer (V-570, JASCO, Japan). Raman spectra were collected at room temperature on a JASCO RFT-6000 spectrometer. X-ray photoelectron spectroscopy (XPS) studies were performed by using a thermo scientific K-ALPHA, XPS, England.

Please cite this article as: R.M. Mohamed, M.W. Kadi, Green synthesis of aniline by phosphorus-doped titanium dioxide polymorphs, Ceramics International (2013), http://dx.doi.org/10.1016/j.ceramint.2013.11.115

2.4. Photoreaction apparatus and procedure

The photocatalytic apparatus consists of two parts. The first part is an annular quartz tube. A 500 W xenon lamp with a maximum emission of approximately 470 nm was used as the visible light source. The wavelength of the visible light is controlled through a cut-off filter ($\lambda > 420$ nm). The lamp is laid in an empty chamber of the annular tube, and running water passes through an inner thimble within the annular tube. Due to continuous cooling, the temperature of the reaction solution is maintained at approximately 30 °C. The second part is a sealed quartz reactor with a diameter of 8.3 cm that is located below the lamp. For each photochemical reaction, a photocatalyst sample (50 mg) was ultrasonically dispersed into a 10 ml NB–CH_3OH solution (1/99 v/v). The initial concentration of NB was 8.13×10^{-4} mol/L. The distance between the light source and the surface of the reaction solution is 11 cm. Nitrogen was passed through the solution for 0.5 h before illumination to remove the dissolved oxygen in the solution to ensure that the photoinduced electrons could be involved in the reduction of NB. After illumination for 4 h, the samples were taken from the reaction suspension, centrifuged at 7000 rpm for 20 min, and finally filtered through a 0.2 μm Millipore filter to remove any residual particles. The filtrate was then analyzed by using a gas chromatography Agilent GC 7890A model: G3440A Gas chromatography using 19091J-413 capillary column (30 m × 0.32 μm × 0.25 μm).

3. Results and discussion

3.1. XRD analysis

The XRD patterns of the concerned systems are displayed in Fig. 1. Upon consideration of the respective XRD diffractograms in Fig.1a, the characteristic peaks of TiO_2 nanoparticles cannot be detected. Moreover; the anatase phase was detected as a major component in the case of a T-36 sample, as shown in Fig. 1b. An examination of the spectra in Fig. 1c reveals the coexistence of the anatase/brookite phase, with the anatase existing as a major phase and the brookite as a minor one. The anatase/brookite binary structures that are produced by increasing the hydrothermal time from 12 to 24 h are likely to be a smaller ratio than the anatase phase (Fig. 1d). As the hydrothermal time is increased from (24 to 36 h), anatase and brookite are partially transformed to rutile, leading to the formation of anatase/brookite/rutile ternary structures (as illustrated in Fig. 1e). In the course of adjusting the hydrothermal time (from 36 to 48 h), the rutile phase becomes the most dominant, with the disappearance of the brookite phase at 48 h (as reported in Fig. 1f).

3.2. Raman analysis

Raman spectroscopy was employed to further confirm the components of the samples because the three titania polymorphs belong to different space groups and exhibit characteristic Raman modes [37]. The bands that peaked at 146, 199, 400, 518, and 639 cm^{-1} are assigned to $E_g(_{v6})$, $E_g(_{v5})$, $B_{1g}(_{v4})$, $A_{1g}(_{v3})$–$B_{1g}(_{v2})$, and $E_g(_{v1})$ modes of anatase [37], respectively. The bands around 248, 322, and 366 cm^{-1} correspond separately to A_{1g}, B_{1g}, and B_{2g} modes of brookite [37]. The bands that peaked at around 446 and 612 cm^{-1} are assigned to E_g and A_{1g} modes of rutile [37]. In the spectrum for T-36 (Fig. 2a), there are no bands around 446 and 612 cm^{-1} that separately correspond to E_g and A_{1g} modes of rutile. Further, there are no bands around 248, 322, and 366 cm^{-1} that separately correspond to A_{1g}, B_{1g}, and B_{2g} modes of brookite and that are indicative of the anatase structure. For the PT-24 sample (Fig. 2b), there are no bands around 446 and 612 cm^{-1} that separately correspond to E_g and A_{1g} modes of rutile, and that are indicative of the anatase/brookite binary structures. For the PT-36 sample (Fig. 2c), three kinds of Raman active modes correspond to the three polymorphs, confirming the anatase/brookite/rutile ternary structures. With respect to the PT-48 sample (Fig. 2d), there are two kinds of Raman active

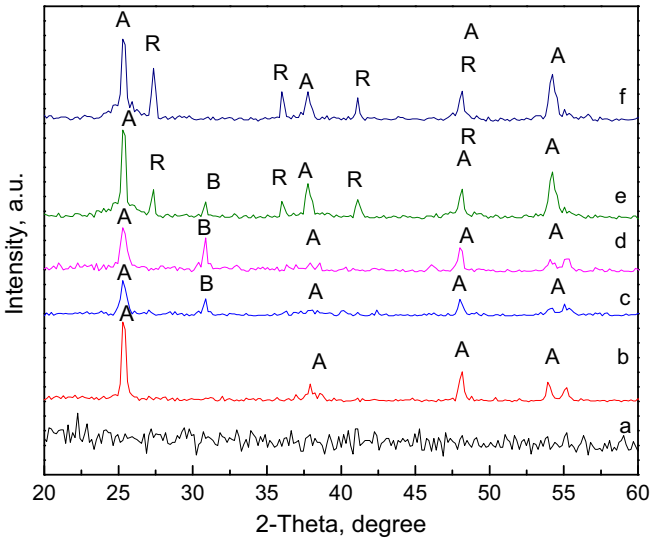

Fig. 1. XRD patterns of the samples (a)TiO_2 nanospheres; (b)T-36, (c) PT-12, (d) PT-24, (e) PT-36 and (f) PT-48.

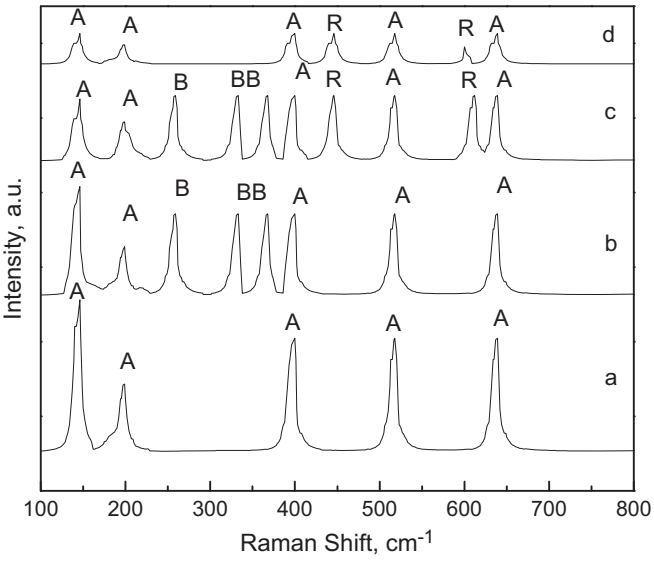

Fig. 2. Raman spectra of the samples: (a)T-36; (b) PT-24; (c) PT-36; and (d) PT-48.

Please cite this article as: R.M. Mohamed, M.W. Kadi, Green synthesis of aniline by phosphorus-doped titanium dioxide polymorphs, Ceramics International (2013), http://dx.doi.org/10.1016/j.ceramint.2013.11.115

modes that correspond to the two polymorphs, confirming the anatase/rutile binary structures, which is in accordance with the XRD analysis.

3.3. TEM observation

TEM analysis prolongates an understanding of the nanostructure morphology within the samples under consideration. It can be observed from Fig. 3 that the TEM images of all of the samples in which Titania nanospheres appear have a mean size of 50 nm (Fig. 3a). After the hydrothermal treatment, TiO_2 nanorods with diameters of 5–10 nm coexist with nanospheres with a mean size of ca. 10 nm (Fig. 3b). The formation of such nanorods are a result of hydrothermal treatment in which the nanotubes begin to smash and fuse together. Inspection of the TEM image that pertains to the PT-36 sample would reveal the existence of nanospheres with sizes of 20–25 nm, which is expected to be an aspect of the dominant nanorods' diameters of 15–30 nm, as displayed in Fig. 3c. Fig. 3d demonstrates the image belongs to the PT-48 sample; keen observation reveals the coexistence of nanowires that have diameters of 4–10 nm within nanospheres with a mean size of 12 nm.

3.4. XPS analysis

The chemical forms of surface elements in the P-doped samples were investigated by XPS analysis. As shown in Fig. 4a, the XPS peaks in the Ti 2p region appear at 458.65 (Ti2p3/2) and 464.45 (Ti 2p1/2) eV for T-36. The binding energy of Ti 2p3/2 shifted to a lower value by 0.10 eV, when compared to that of PT-36 (458.75 eV). The decrease in binding energy of Ti2p after P-doping suggests the change in the electronic environment of Ti ions, where partial electrons transfer from P to Ti; hence, electron density on the Ti increases because of the lower electronegativity of phosphor in comparison to oxygen [39]. This means that phosphor incorporates into the TiO_2 lattice and substitutes for oxygen to form the O–Ti–P structure [39], which is further confirmed by P 2p regions (Fig. 4b). The XPS spectrum of P 2p in Fig. 4b consists of a double peak of P 2p3/2 and P 2p1/2. The binding energy of P 2p3/2 in PT-36 located at 134.15 eV indicates the existence of P^{5+}. This value is also different from that of P^{5+} in Na_3PO_4-impregnated TiO_2, which is located at 133.35 eV. As the ionic radii for Ti^{4+} and P^{5+} are not very close (0.67 and 0.38 Å, respectively, in an environment of coordination number 6), P^{5+} species are not

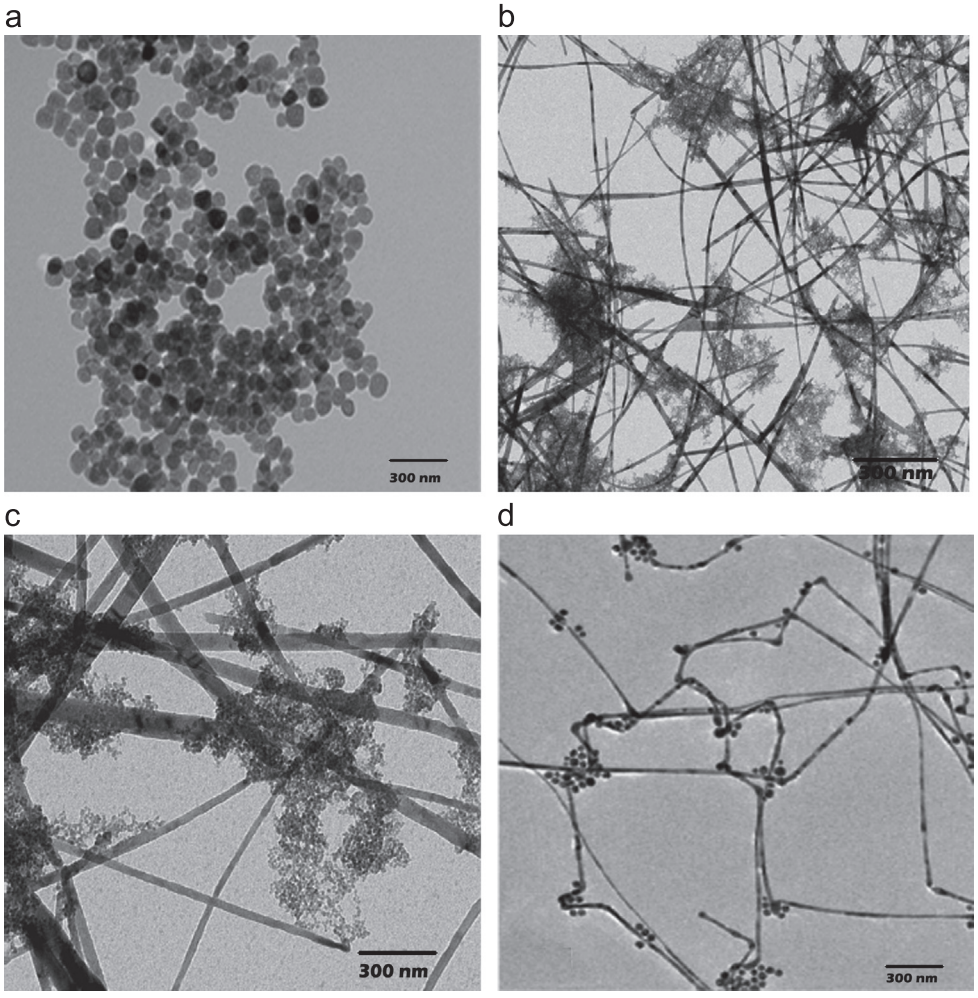

Fig. 3. TEM images of the samples: (a)T-36; (b) PT-24; (c) PT-36; and (d) PT-48.

Please cite this article as: R.M. Mohamed, M.W. Kadi, Green synthesis of aniline by phosphorus-doped titanium dioxide polymorphs, Ceramics International (2013), http://dx.doi.org/10.1016/j.ceramint.2013.11.115

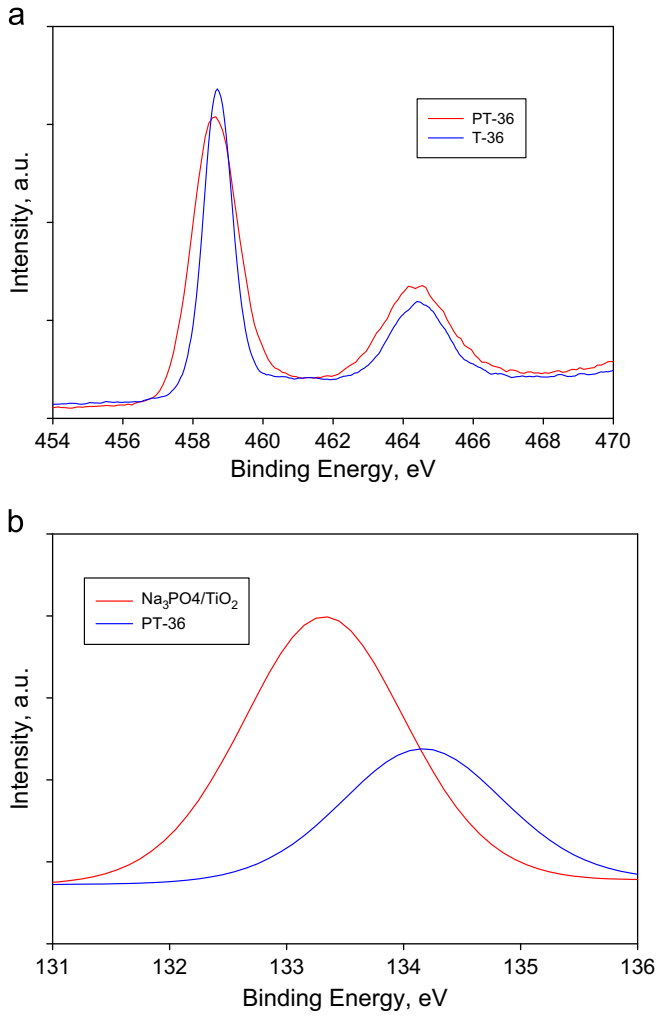

Fig. 4. (a) XPS spectra of the T-36 and PT-36 samples for Ti2p region and (b) XPS spectra of the T-36 and PT-36 samples for P 2p region.

Table 1
Physicochemical properties of TiO_2 and P-doped TiO_2 samples.

Sample	Anatase (%)	Brookite (%)	Rutile (%)	Band gap energy (eV)	BET (m^2/g)
T-36	99.2	0.8	–	3.1	55.0
PT-12	95.5	4.5	–	2.85	66.5
PT-24	85.8	14.2	–	2.48	77.4
PT-36	84.6	3.9	11.5	2.33	62.1
PT-48	61.5	–	38.5	2.22	49.7

likely to exist in the bulk with high concentration. Thus, we suggest that doped P may exist on or near the surface region in an octahedral environment by replacing part of Ti^{4+}, rather than as PO_4^{3-} in a tetrahedral environment.

3.5. Analysis of surface area

The values of the specific surface areas, S_{BET} ($m^2\ g^{-1}$) of the concerned systems, were calculated by applying the BET equation for TiO_2 and P-doped TiO_2; both catalytic systems under investigation are cited in Table 1. Following up the variation of S_{BET} values of both concerned systems, two points can be raised.

- The S_{BET} values increased from 55 to 77.4 m^2/g with the increased content of the brookite structure.
- The drop in S_{BET} values from 77.4 to 49.7 m^2/g upon raising the content of rutile from 0% to 38.5%.

3.6. UV–vis diffuse reflectance spectra

Fig. 5 shows the diffused absorbance spectra of the samples. It is found that the absorption in the range of 435–562 nm for the P-doped samples is higher in intensity than that for the undoped T-36 sample. The band gap for the T-36, PT-12, PT-24, PT-36, and PT-48 is calculated to be 3.1, 2.85, 2.48, 2.33, and 2.22 eV, respectively, according to the following formula:

$$E_g(ev) = \frac{1240}{\lambda_g}$$

The band gap wavelength (λ_g, nm) is obtained by extrapolating the wavelength edge of the peak in absorbance in relation to the zero line from diffuse reflectance spectra. The band gaps of the P-doped samples decrease with phosphor doping and with the gradual increase in rutile content. This indicates that rutilation of the ternary and binary TiO_2 structures plays a significant role in shifting the absorption edge toward the visible light region [39].

3.7. Photocatalytic activity

Photocatalytic activities of the prepared samples were studied by the photocatalytic production of aniline (AN) via nitrobenzene (NB) reduction under visible light irradiation. Gas chromatogram (GC) results showed that the main products

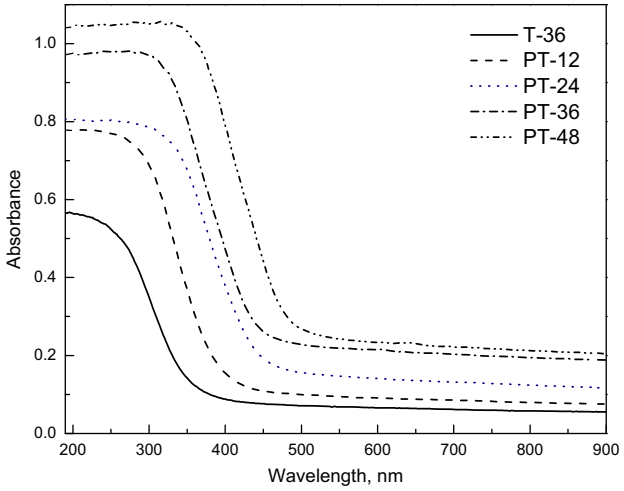

Fig. 5. UV–vis spectra of the samples.

Please cite this article as: R.M. Mohamed, M.W. Kadi, Green synthesis of aniline by phosphorus-doped titanium dioxide polymorphs, Ceramics International (2013), http://dx.doi.org/10.1016/j.ceramint.2013.11.115

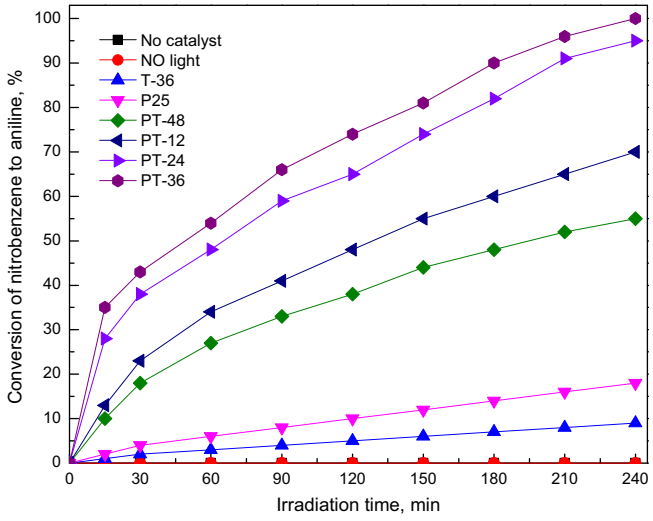

Fig. 6. Conversion of nitrobenzene to aniline, % of prepared samples.

were nitrosobenzene and aniline. No nitrosobenzene or aniline was detected in the absence of only catalysts or light irradiation. It is found that all of the phosphor-doped samples bear enhanced photocatalytic activity in comparison to the undoped sample (Fig. 6). This result is partially due to phosphors doping and energy band matching between titania polymorphs that can suppress the recombination of photo-induced electron–hole pairs by modifying the electronic properties of TiO_2 [37]. The commercial P_{25} that consists of the anatase/rutile binary structure has been widely employed for comparison to evaluate the properties of a photocatalyst. The photocatalytic efficiencies of PT-12, PT-24, PT-36, and PT-48 samples are 3.8, 5.3, 5.5, and 3.0 times, respectively, that of P_{25} under visible light irradiation for 4 h because of its large band gap. This finding can also be assigned to phosphor doping and to one-dimensional anatase nanowires that serve as electron highways to facilitate the efficient separation of the charge carries [41]. Although the sample of PT-24 with anatase/brookite structures has the largest BET surface area, the sample of PT-36 with ternary titania polymorphs having a medium BET surface area shows the highest photocatalytic efficiency. This data reveals that the existence of rutile plays an important role in contributing to the visible light's catalytic activity. However, for the PT-48 sample, with increasing rutile content that is comparable to the anatase content, the photo-catalytic efficiency decreases in comparison to that of PT-36. This result can be assigned to the larger amount of the rutile phase that has a higher electron–hole recombination rate, and to the decrease in the amount of more photoactive anatase phase and surface area [39].

3.8. Photochemical stability

For the practical applications of a photocatalyst, two factors that are related to recycling should be considered, such as the ease of separation from a solution, as well as the stability in maintaining high activity and in resisting photocorrosion after long-term use. In this research, the PT-36 sample that has anatase nanowires can be easily separated from an aqueous solution. Therefore, the PT-36 sample was selected for reuse five times in order to test its stability (Fig. 7). After five catalysis cycles to

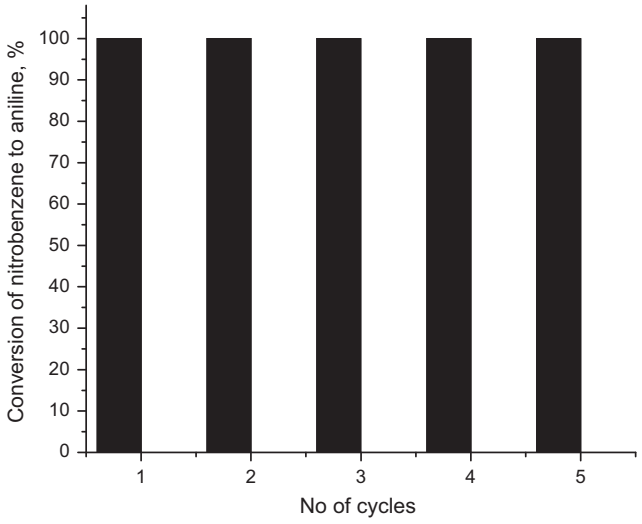

Fig. 7. Recycling test for the PT-36 sample.

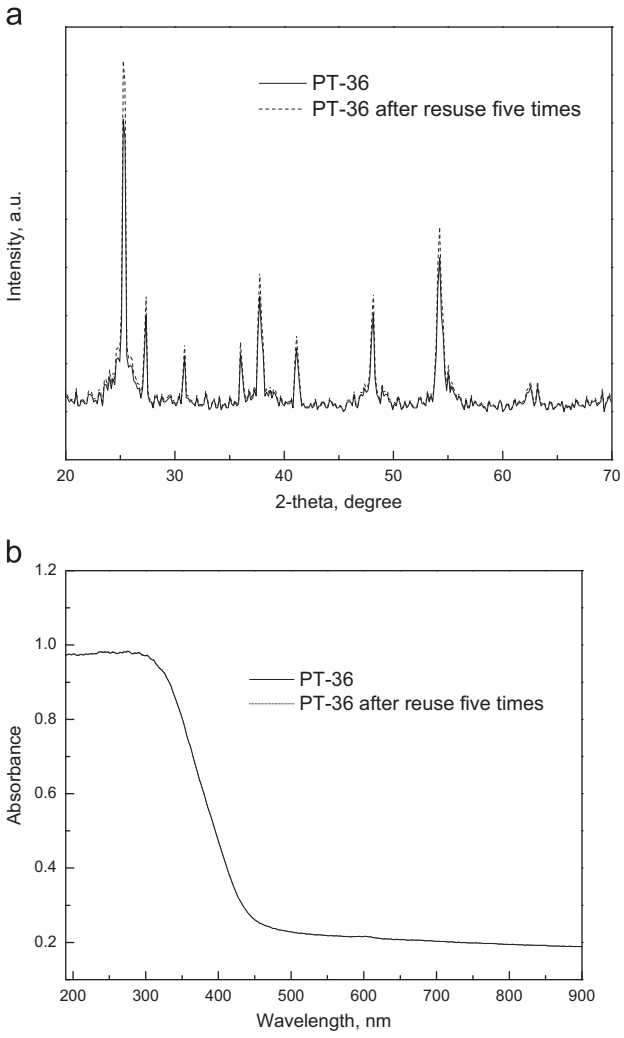

Fig. 8. (a). XRD patterns of PT-36 and PT-36 after reuse five times. (b). UV–vis spectra of PT-36 and PT-36 after reuse five times.

Please cite this article as: R.M. Mohamed, M.W. Kadi, Green synthesis of aniline by phosphorus-doped titanium dioxide polymorphs, Ceramics International (2013), http://dx.doi.org/10.1016/j.ceramint.2013.11.115

reduce nitrobenzene, the PT-36 sample with ternary titania polymorphs does not show dramatic deactivation. This result is indicative of high photostability of the catalyst, in concert with the XRD and UV–vis results (Fig. 8a and b). The results reveal that the PT-36 sample nearly remains unchanged in crystal phase, composition, and absorption after reuse five times, which indicates its high stability and suitability for recycling.

3.9. Mechanisms

Gas chromatogram (GC) results showed that the main products were nitrosobenzene and aniline. The mechanisms of the photocatalytic reduction of NB over the PT-36 sample is discussed as follows [43]: (1) Production of photogenerated hole–electron pairs. When irradiated by photos with energy equal or that are larger than its band gap, electrons transfer from the valence band to the conduction band, thus producing oxidative photogenerated valence holes (h^+) and reductive conduction electrons (e^-) (Eqs. (1) and (2)) Photogenerated holes and electrons without recombination move to the photocatalyst's surface. (3) Chemical reactions between photogenerated carriers and adsorbents. The holes are captured by a CH_3OH solvent, producing HCHO oxide and reductive H (Eqs. (2) and (3)). NB is reduced by photogenerated electrons and H, therefore producing nitrosobenzene and aniline (Eq. (4)).

$$TiO_2 + \text{Visible light} \longrightarrow TiO_2\ (e^- + h^+) \quad (1)$$

$$CH_3OH + h^+ \longrightarrow CH_3O^{\bullet} + {}^{\bullet}CH_2OH \quad (2)$$

$$CH_3O^{\bullet} + {}^{\bullet}CH_2OH \longrightarrow 2H^{\bullet} + 2HCHO \quad (3)$$

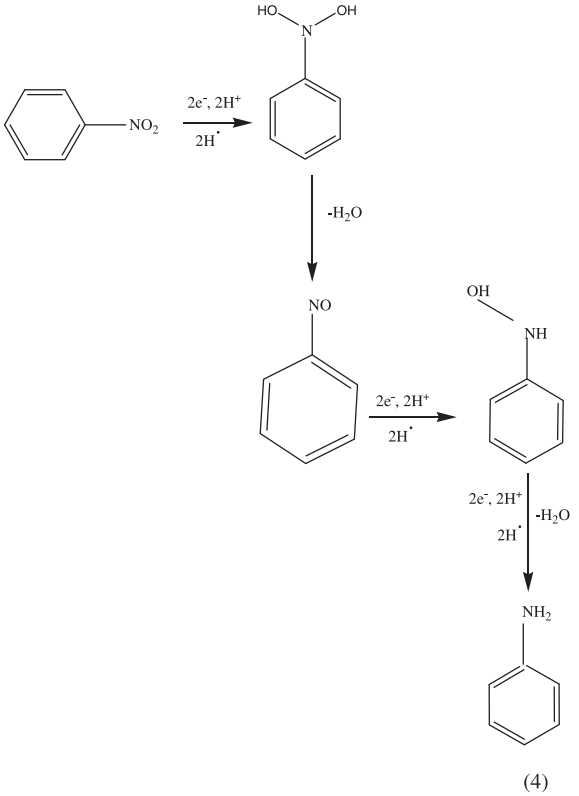

(4)

4. Conclusion

In summary, the controlled synthesis of phosphor-doped titania nanostructures with binary and/or ternary polymorphs have been achieved via a hydrothermal method. In addition, the phosphor-doped catalysts show enhanced catalytic ability for the green synthesis of aniline by the photocatalytic reduction of nitrobenzene (i.e., in comparison to P_{25} and the undoped counterpart). The PT-36 sample has high photostability after reuse five times for the photocatalytic reduction of nitrobenzene. The photocatalytic efficiency of the fifth cycle for the PT-36 sample remains 5.5 times that of P_{25} that was used in the first run. This new type of TiO_2 nanostructure presents a promising candidate for application in photocatalysis, photochemistry, sensors, and solar cells.

References

[1] A. Corma, P. Concepcion, P. Serna, A different reaction pathway for the reduction of aromatic nitro compounds on gold catalysts, Angew. Chem. Int. Ed. 46 (2007) 7266–7269.
[2] J. Wang, Z. Yuan, R. Nie, Z. Hou, X. Zheng, Hydrogenation of nitrobenzene to aniline over silica gel supported nickel catalysts Ind, Eng. Chem. Res. 49 (2010) 4664–4669.
[3] S.-P. Lee, Y.-W. Chen, Nitrobenzene hydrogenation on Ni–P, Ni–B and Ni–P–B ultrafine materials, J. Mol. Catal. A: Chem. 152 (2000) 213–223.
[4] H. Li, Q. Zhao, Y. Wan, W. Dai, M. Qiao, Self-assembly of mesoporous Ni–B amorphous alloy catalysts, J. Catal. 244 (2006) 251–254.
[5] S.O. Flores, O. Rios-Bernij, M.A. Valenzuela, I. Córdova, R. Gómez, R. Gutiérrez, Photocatalytic reduction of nitrobenzene over titanium dioxide: by-product identification and possible pathways, Topics Catal. 44 (2007) 507–511.
[6] S. Fuldner, P. Pohla, H. Bartling, S. Dankesreiter, R. Stadler, M. Gruber, A. Pfitzner, B. Konig, Selective photocatalytic reductions of nitrobenzene derivatives using $PbBiO_2-X$ and blue light, Green Chem. 13 (2011) 640–643.
[7] J.L. Ferry, W.H. Glaze, Photocatalytic reduction of nitro organics over illuminated titanium dioxide: role of the TiO_2 surface, Langmuir 14 (1998) 3551–3555.
[8] S. Chen, H. Zhang, X. Yu, W. Liu, Photocatalytic reduction of nitrobenzene by titanium dioxide powder, Chin, J. Chem. 28 (2010) 21–26.
[9] F. Mahdavi, T.C. Bruton, Y. Li, Photoinduced reduction of nitro compounds on semiconductor particles, J. Org. Chem. 58 (1993) 744–746.
[10] J.L. Ferry, W.H. Glaze, Photocatalytic reduction of nitroorganics over illuminated titanium dioxide: electron transfer between excited-state TiO_2 and nitroaromatics, J. Phys. Chem. B 102 (1998) 2239–2244.
[11] G. Liu, X. Li, J. Zhao, S. Horikoshi, H. Hidaka, Photooxidation mechanism of dye alizarin red in TiO_2 dispersions under visible illumination: an experimental and theoretical examination, J. Mol. Catal. A: Chem. 153 (2000) 221–229.
[12] H.-P. Dai, K.-K. Shiu, Voltammetric behavior of alizarin red S adsorbed on electrochemically pretreated glassy carbon electrodes, Electrochim. Acta 43 (1998) 2709–2715.
[13] S.D. Rychnovsky, R. Vaidyanathan, T. Beauchamp, R. Lin, P.J. Farmer, AM1-SM2 calculations model the redox potential of nitroxyl radicals such as TEMPO, J. Org. Chem. 64 (1999) 6745–6749.
[14] M. Zhang, C. Chen, W. Ma, J. Zhao, Visible-light-induced aerobic oxidation of alcohols in a coupled photocatalytic system of dye-sensitized TiO_2 and TEMPO, Angew. Chem. Int. Ed. 120 (2008) 9876–9879.
[15] S. Balasubramanian, Luminescence behavior of tetraaza macrocylic nickel (II) complexes and non-linear Stern–Volmer quenching, J. Lumin. 106 (2004) 69–76.

Please cite this article as: R.M. Mohamed, M.W. Kadi, Green synthesis of aniline by phosphorus-doped titanium dioxide polymorphs, Ceramics International (2013), http://dx.doi.org/10.1016/j.ceramint.2013.11.115

[16] M.Y. Abdelaal, R.M. Mohamed, Novel Pd/TiO_2 nanocomposite prepared by modified sol–gel method for photocatalytic degradation of methylene blue dye under visible light irradiation, J. Alloys Compd. 576 (2013) 201–207.

[17] R.M. Mohamed, E.S. Aazam, H_2 production with low CO selectivity from photocatalytic reforming of glucose on Ni/TiO_2–SiO_2, Chin. J. Catal. 33 (2) (2012) 247–253.

[18] R.M. Mohamed, UV-assisted photocatalytic synthesis of TiO_2-reduced graphene oxide with enhanced photocatalytic activity in decomposition of Sarin in gas phase, Desalinat. Water Treat. 50 (2012) 147–156.

[19] R.M. Mohamed, D.L. McKinney, W.M. Sigmund, Enhanced nanocatalysts, Mater. Sci. Eng. R 73 (2012) 1–13.

[20] R.M. Mohamed Elham, S. Aazam, Photocatalytic oxidation of carbon monoxide over NiO/SnO_2 nanocomposites under UV irradiation, J. Nanotechnol. 2012 (2012) 9 Article ID 794874.

[21] R.M. Mohamed, Elham S. Aazam, Preparation and characterization of platinum doped porous titania nanoparticles for photocatalytic oxidation of carbon monoxide, J. Alloys Compd. 509 (2011) 10132–10138.

[22] R.M. Mohamed, I.A. Mkhalid, Characterization characterization and catalytic properties of nano-sized Ag metal catalyst on TiO_2–SiO_2 Synthesized by Photo-Assisted Deposition (PAD) and impregnation methods, J. Alloys Compd. 501 (2010) 301–306.

[23] R.M. Mohamed, I.A. Mkhalid, The effect of rare earth dopants on the structure, surface texture and photocatalytic properties of TiO_2–SiO_2 prepared by sol–gel method, J. Alloys Compd. 501 (2010) 143–147.

[24] R.M. Mohamed, E.S. Baeissa, Mordenite encapsulated with Pt–TiO_2: characterization and applications for photocatalytic degradation of direct blue dye, J. Alloys Compd. 558 (2013) 68–72.

[25] R.M. Mohamed, E.S. Baeissa, Preparation and characterization of Pd–TiO_2-hydroxyapatite nanoparticles for the photocatalytic degradation of cyanide under visible light, Appl. Catal. A 464–465 (2013) 218–224.

[26] A.K. Geim, K.S. Novoselov, The rise of graphene, Nat. Mater. 6 (2007) 183–191.

[27] L. Cui, Y. Wang, M. Niu, G. Chen, Y. Cheng, Synthesis and visible light photocatalysis of Fe-doped TiO_2 mesoporous layers deposited on hollow glass microbeads, J. Solid State Chem. 182 (2009) 2785–2790.

[28] J.M. Herrmann, H. Tahiri, Y. Ait-Ichou, G. Lassaletta, A.R.Gonza´ lez-Elipe, A. Ferna´ ndez, Characterization and photocatalytic activity in aqueous medium of TiO_2 and Ag–TiO_2 coatings on quartz, Appl.Catal. B13 (1997) 219–228.

[29] S.K. Mohapatra, N. Kondamudi, S. Banerjee, M. Misra, Functionalization of self-organized TiO_2 nanotubes with Pd nanoparticles for photocatalytic decomposition of dyes under solar light illumination, Langmuir 24 (2008) 11276–11281.

[30] K. Shankar, J.I. Basham, N.K. Allam, O.K. Varghese, G.K. Mor, X. Feng, M. Paulose, J.A. Seabold, K.S. Choi, C.A. Grimes, Recent Advances in the use of TiO_2 nanotube and nanowire arrays for oxidative photoelectrochemistry, J. Phys. Chem. C 113 (2009) 6327–6359.

[31] N. Serpone, P. Maruthamuthu, P. Pichat, E. Pelizzetti, H. Hidaka, Exploiting the interparticle electron transfer process in the photocatalysed oxidation of phenol, 2-chlorophenol and pentachlorophenol: chemical evidence for electron and hole transfer between coupled semiconductors, J. Photochem. Photobiol. A 85 (1995) 247–255.

[32] B. Gao, Y.J. Kim, A.K. Chakraborty, W.I. Lee, Efficient decomposition of organic compounds with $FeTiO_3$/TiO_2 heterojunction under visible light irradiation, Appl. Catal. B 83 (2008) 202–207.

[33] Y.J. Kim, B. Gao, S.Y. Han, M.H. Jung, A.K. Chakraborty, T. Ko, C. Lee, W.I. Lee, Heterojunction of $FeTiO_3$ nanodisc and TiO_2 nanoparticle for a novel visible light photocatalyst, J. Phys. Chem. C 113 (2009) 19179–19184.

[34] L. Kavan, M. Gratzel, S.E. Gilbert, C. Klemenz, H.J. Scheel, Electrochemical and photoelectrochemical investigation of single-crystal anatase, J. Am. Chem. Soc. 118 (1996) 6716–6723.

[35] J.C. Yu, L. Zhang, J. Yu, Direct sonochemical preparation and characterization of highly active mesoporous TiO_2 with a bicrystalline framework, Chem. Mater. 14 (2002) 4647–4653.

[36] G. Tian, H. Fu, L. Jing, B. Xin, K. Pan, Preparation and characterization of stable biphase TiO_2 photocatalyst with high crystallinity, large surface area, and enhanced photoactivity, J. Phys. Chem. C 112 (2008) 3083–3089.

[37] J.G. Li, T. Ishigaki, X. Sun, Anatase, brookite, and rutile nanocrystals via redox reactions under mild hydrothermal conditions: phase-selective synthesis and physicochemical properties, J. Phys. Chem. C 111 (2007) 4969–4976.

[38] D.C. Hurum, A.G. Agrios, K.A. Gray, T. Rajh, M.C. Thurnauer, Explaining the enhanced photocatalytic activity of degussa P25 Mixed-phase TiO_2 using EPR, J. Phys. Chem. B 107 (2003) 4545–4549.

[39] V. Etacheri, M.K. Seery, S.J. Hinder, S.C. Pillai, Highly visible light active $TiO_{2-x}N_x$ heterojunction photocatalysts, Chem. Mater. 22 (2010) 3843–3853.

[40] A.V. Emeline, L.G. Smirnova, G.N. Kuzmin, L.L. Basov, N. Serpone, Spectral dependence of quantum yields in gas–solid heterogeneous photosystems: Influence of anatase/rutile content on the photostimulated adsorption of dioxygen and dihydrogen on titania, J. Photo-Chem. Photobiol. A 148 (2002) 97–102.

[41] N. Wu, J. Wang, D. Nyago Tafen, H. Wang, J. Zheng, J.P. Lewis, X. Liu, S.S. Leonard, A. Manivannan, Shape-enhanced photocatalytic activity of single-crystalline anatase TiO_2 (101) nanobelts, J. Am. Chem. Soc. 132 (2010) 6679–6685.

[42] H. Zhang, J.F. Banfield, Understanding polymorphic phase transformation behavior during growth of nanocrystalline aggregates: insights from TiO_2, J. Phys. Chem. B 104 (2000) 3481–3487.

[43] A.H. Qusti, R.M. Mohamed, M. Abdel Salam, Photocatalytic synthesis of aniline from nitrobenzene using Ag-reduced graphene oxide nanocomposite, Ceram. Int. In press, ⟨http://dx.doi.org/10.1016/j.ceramint.2013.10.144⟩.

Please cite this article as: R.M. Mohamed, M.W. Kadi, Green synthesis of aniline by phosphorus-doped titanium dioxide polymorphs, Ceramics International (2013), http://dx.doi.org/10.1016/j.ceramint.2013.11.115